Stopping, straggling, and blooming of directed energetic electrons in hydrogenic and arbitrary-*Z* plasmas

C. K. Li and R. D. Petrasso
Plasma Science and Fusion Center, Massachusetts Institute of Technology, Cambridge, Massachusetts 02139, USA
(Received 1 November 2004; published 18 January 2006)

From fundamental principles, the interaction of directed energetic electrons with hydrogenic and arbitrary-*Z* plasmas is analytically modeled. The effects of stopping, straggling, and beam blooming, a consequence of scattering and energy loss, are rigorously treated from a unified approach. Enhanced energy deposition occurs in the latter portion of the penetration and is inextricably linked to straggling and blooming. These effects, which have a strong *Z* dependence, will be important in evaluating the requirements of fast ignition and tolerable levels of electron preheat.

DOI: 10.1103/PhysRevE.73.016402 PACS number(s): 52.55.Pi, 52.25.Tx, 52.40.Mj, 52.50.Gj

A basic problem in plasma physics is the interaction and energy loss of energetic charged particles in plasmas [1–3], including the effects of penetration, longitudinal straggling, and lateral blooming. This problem has traditionally focused on ions (i.e., protons, α's, etc.), either in the context of heating and/or ignition in, for example, inertially confined plasmas (ICF) [3–7]; or the use of these particles for diagnosing implosion dynamics [8]. More recently, prompted in part by the concept of fast ignition (FI) for ICF [9], workers have begun considering energy deposition from relativistic electrons in deuterium-tritium (DT) plasmas [9–14]. In this context, we recently calculated the mean penetration and stopping power for energetic electrons interacting with a uniform hydrogenic plasma of arbitrary density and temperature. Therein, the randomizing effect of electron scattering, which has a cumulative effect of bending the path of the electrons away from their initial direction, was linked to an energy loss [14]. In this paper we present calculations which show the effects of longitudinal straggling and transverse blooming, and their inextricable relationship with enhanced electron energy deposition. We demonstrate that, while the initial penetration results in an approximate uniform energy deposition, the latter penetration has mutual couplings of energy loss, straggling, and blooming that lead to an extended region of enhanced, nonuniform energy deposition. This present work is important for quantitatively evaluating the energy deposition in several current problems. In the case of FI, for example, there have been no evaluations which have treated either straggling or blooming upon the energy deposition, without which there can be no confident assessment of ignition requirements. The calculations herein, therefore, form the foundation for a baseline, at the very least, or an accurate assessment, at the very most, by which to evaluate these effects upon FI. In addition to FI, these calculations are sufficiently general to be of relevance to other current problems, such as the fast electron preheat [15] in ICF, or to the energy deposition and penetration of relativistic electrons in astrophysical jets [16].

To delineate these processes, we calculate the different moments by analytically solving an integrodifferential diffusion equation [17], thereby determining the angular and spatial distributions of the scattered electrons.

$$\frac{\partial f}{\partial s} + \mathbf{v}\cdot\nabla f = n_i \int [f(\mathbf{x},\mathbf{v}',s) - f(\mathbf{x},\mathbf{v},s)]\sigma(|\mathbf{v}-\mathbf{v}'|)d\mathbf{v}', \tag{1}$$

where $f(\mathbf{x},\mathbf{v},s)$ is the electron distribution function; n_i is the number density of fully ionized, uniform time invariant background plasma ions of charge Z; $\mathbf{x}$ is the position where scattering occurs; $\sigma=\sigma_{ei}+Z\sigma_{ee}$ is the total scattering cross section with σ_{ei} the Rutherford *e-ion* cross section [18], and σ_{ee} the Møller *e-e* cross section [19]. We solve this equation in cylindrical coordinates with the assumption that the scattering is azimuthally symmetric. After expanding the distribution in spherical harmonics and substituting into Eq. (1), two differential equations for the longitudinal and lateral distributions are obtained. For the longitudinal distribution:

$$\frac{\partial F^n_{\ell m}(s)}{\partial s} + \kappa_\ell(s)F^n_{\ell m}(s) - n\left[\frac{\ell}{\sqrt{4\ell^2-1}}F^{n-1}_{\ell-1,m}(s) + \frac{\ell+1}{\sqrt{4(\ell+1)^2-1}}F^{n-1}_{\ell+1,m}(s)\right] = 0. \tag{2}$$

And for lateral distribution:

$$\frac{\partial F^n_{\ell m}(s)}{\partial s} + \kappa_\ell(s)F^n_{\ell m}(s) - \frac{n}{2}\left[\sqrt{\frac{(\ell+m)(\ell+m-1)}{4\ell^2-1}}F^{n-1}_{\ell-1,m-1}(s) + \sqrt{\frac{(\ell+m+2)(\ell+m+1)}{4(\ell+1)^2-1}}F^{n-1}_{\ell+1,m+1}(s) - \sqrt{\frac{(\ell-m)(\ell-m-1)}{4\ell^2-1}}F^{n-1}_{\ell-1,m+1}(s) - \sqrt{\frac{(\ell-m+2)(\ell-m+1)}{4(\ell+1)^2-1}}F^{n-1}_{\ell+1,m+1}(s)\right] = 0, \tag{3}$$

where the moments are defined as $F^n_{\ell m}(s)=\int_{-\infty}^{\infty}x_j^n f_{\ell m}(\mathbf{x},s)d\mathbf{x}$, n is the order of the moment, and $j=1,2,3$ represents x,y,z, respectively.

TABLE I. Interactions of 1 MeV electrons with DT, beryllium, aluminum, and copper plasmas, assuming plasma $T_e=5$ keV and $n_e=7.2\times10^{25}$ in every case. For Cu plasma, bremsstrahlung loses are about 5%, and are ignored.

Z	ρ (g/cm^3)	R (μm)	$\langle x\rangle$ (μm)	$\rho\langle x\rangle$ (g/cm^2)	Σ_R (μm)	Σ_B (μm)	$\Sigma_R/\langle x\rangle$	$\Sigma_B/\langle x\rangle$
1	300	17.9	13.9	0.42	2.7	4.7	0.19	0.33
4	271	17.9	10.6	0.29	3.8	5.4	0.36	0.51
13	249	17.9	6.3	0.16	4.2	5.1	0.67	0.81
29	265	17.9	3.7	0.10	3.7	4.2	1.0	1.14

$$\kappa_\ell(s)=n_i\int\left(\frac{d\sigma}{d\Omega}\right)[1-P_\ell(\cos\theta)]d\Omega, \tag{4}$$

where $(d\sigma/d\Omega)$ is the total differential cross section of *e-ion* and *e-e* scattering [18,19,14], $P_\ell(\cos\theta)$ are the Legendre polynomials, and $\kappa_\ell(s)$ are directly related to the basic transport cross sections [2]. Equations (2) and (3) are coupled to adjacent orders in n, and are solved with the boundary condition

$$F^n_{\ell m}(s)=\sqrt{(2\ell+1)/4\pi}\,\delta_{m0}\delta_{n0}\exp\left(-\int_0^S\kappa_\ell(s')ds'\right),$$

where $F^n_{\ell m}(0)=0$ for $n\neq0$. Solving for κ_1 and κ_2

$$\kappa_1=4\pi n_i\left(\frac{r_0}{\gamma\beta^2}\right)^2\left[Z^2\ln\Lambda^{ei}+\frac{4(\gamma+1)^2}{(2^{\sqrt{(\gamma+1)/2}})^4}Z\ln\Lambda^{ee}\right]; \tag{5}$$

and

$$\kappa_2=12\pi n_i\left(\frac{r_0}{\gamma\beta^2}\right)^2\left[Z^2\left(\ln\Lambda^{ei}-\tfrac{1}{2}\right)+\frac{4(\gamma+1)^2}{(2^{\sqrt{(\gamma+1)/2}})^4}Z\left(\ln\Lambda^{ee}-\tfrac{1}{2}\right)\right]. \tag{6}$$

κ_1 is related to the slowing-down cross section [2], which characterizes the loss of directed velocity in the scattering; and κ_2 is related to the deflection cross section which represents the mean-square increment in the transverse electron velocity during the scattering process [2]. $\beta=v/c$ and $\gamma=(1-\beta^2)^{-1/2}$; $r_0=e^2/m_0c^2$ is the classical electron radius. The arguments of the Coulomb logarithm are $\Lambda^{ei}=\lambda_D/b^{ei}_{\min}$, and $\Lambda^{ee}=\lambda_D/b^{ee}_{\min}$, where λ_D is the Debye length, and $b^{ei}_{\min}$ ($b^{ee}_{\min}$) is the larger of b^{ei}_q (b^{ee}_q) and $b^{ei}_\perp$ ($b^{ee}_\perp$) [14]. b^{ei}_q and b^{ei}_q are approximately the electron deBroglie wavelength, and $b^{ei}_\perp=Zr_0/\gamma\beta^2$ and $b^{ee}_\perp\approx2(\gamma+1)r_0/[(2^{\sqrt{(\gamma+1)/2}})^2\gamma\beta^2]$ are the impact parameters for 90° scattering of electrons off ions or electrons off electrons [14]. The angular distribution function is obtained

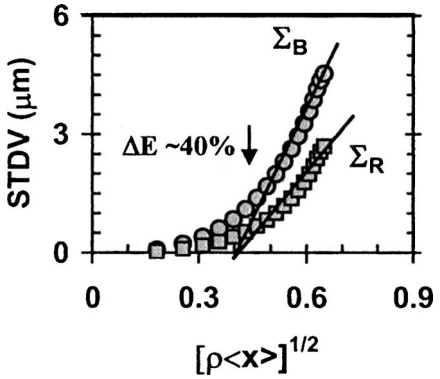

FIG. 1. Σ_R and Σ_B are plotted as a function of the square root of the penetration for a 1-MeV electron beam in a DT plasma of 300 g/cm^3 at 5 keV. When the electrons have lost more than ~40% of their initial energy, both Σ_R and Σ_B are approximately proportional to $\sqrt{\rho\langle x\rangle}$.

$$f(\theta,E)=\frac{1}{4\pi}\sum_{\ell=0}^{\infty}(2\ell+1)P_\ell(\cos\theta)\times\exp\left[-\int_{E_0}^{E}\kappa_\ell(E')\left(\frac{dE'}{ds}\right)^{-1}dE'\right], \tag{7}$$

from which $\langle P_\ell(\cos\theta)\rangle$ is calculated

$$\langle P_\ell(\cos\theta)\rangle=\exp\left\{-\int_{E_0}^{E}\kappa_\ell(E')\left(\frac{dE'}{ds}\right)^{-1}dE'\right\}; \tag{8}$$

where dE/ds is plasma stopping power taken from Ref. 14,

$$\frac{dE}{ds}=-\frac{2\pi r_0^2m_0c^2n_iZ}{\beta^2}\left[\ln\left(\frac{(\gamma-1)\lambda_D}{2\sqrt{2}\gamma r_0}\right)^2+1+\frac{1}{8}\left(\frac{\gamma-1}{\gamma}\right)^2-\left(\frac{2\gamma-1}{\gamma}\right)\ln2+\ln\left(\frac{1.123\beta}{\sqrt{2kT_e/m_0c^2}}\right)^2\right], \tag{9}$$

which consists of contributions from binary interactions with

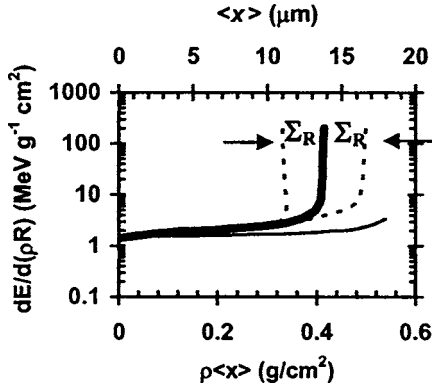

FIG. 2. The stopping power is plotted as a function of the electron penetration for 1-MeV electrons in a DT plasma ($\rho=300$ g/cm^3 and $T_e=5$ keV). The heavy solid line represents the mean energy loss, while the two dashed lines indicate the straggling range over which the energy is effectively spread. (In this plot, important contributions from blooming are not included; see text.) The thin line illustrates the continuous slowing-down approximation [14], and is directly related to R, the total path length.

TABLE II. Interactions of 1 MeV electrons with DT plasmas of various densities.

ρ (g/cm^3)	$\langle x\rangle$ (μm)	$\rho\langle x\rangle$ (g/cm^2)	Σ_R (μm)	Σ_B (μm)	$\Sigma_R/\langle x\rangle$	$\Sigma_B/\langle x\rangle$
100	39.7	0.40	8.0	13.4	0.20	0.34
300	13.9	0.42	2.7	4.7	0.19	0.33
1000	4.5	0.45	0.9	1.5	0.20	0.33

plasma electrons and from plasma oscillations. From these results, we solve Eqs. (2) and (3), and evaluate basic moments required for the calculation of the longitudinal and lateral distributions:

$$\langle x\rangle = \int_{E_0}^{E} \langle P_1(\cos\theta)\rangle \left(\frac{dE'}{ds}\right)^{-1} dE', \tag{10}$$

which was evaluated in a previous work for the case of 1-MeV electron stopping in a DT 300 g/cm^3 plasma at 5 keV. This results in a penetration ($\langle x\rangle$) of 13.9 μm [14]

$$\langle x^2\rangle = \frac{2}{3}\int_{E_0}^{E} \langle P_1(\cos\theta)\rangle \left(\frac{dE'}{ds}\right)^{-1} \times \left(\int_{E_0}^{E'} \frac{1+2\langle P_2(\cos\theta)\rangle}{\langle P_1(\cos\theta)\rangle}\left(\frac{dE''}{ds}\right)^{-1} dE''\right) dE'. \tag{11}$$

Because of azimuthally symmetry, $\langle y\rangle = \langle z\rangle = 0$, and

$$\langle y^2\rangle = \langle z^2\rangle = \frac{2}{3}\int_{E_0}^{E} \langle P_1(\cos\theta)\rangle \left(\frac{dE'}{ds}\right)^{-1} \times \left(\int_{E_0}^{E'} \frac{1-\langle P_2(\cos\theta)\rangle}{\langle P_1(\cos\theta)\rangle}\left(\frac{dE''}{ds}\right)^{-1} dE''\right) dE'. \tag{12}$$

In evaluating Eqs. (10)–(12), one needs to evaluate $\langle P_1(\cos\theta)\rangle$ and $\langle P_2(\cos\theta)\rangle$, the first and second order mean Legendre polynomials. Substituting Eqs. (5) and (6), respectively, into Eq. (8), and using the stopping power [Eq. (9)], both quantities are readily calculated.

TABLE III. Interactions of 0.1–10 MeV electrons with DT plasma of 300 g/cm^3. ΔE is the percentage of energy loss when Σ_R and Σ_B are starting to become significant, as illustrated in Fig. 1.

E_0 (MeV)	ΔE (%)	$\langle x\rangle$ (μm)	$\rho\langle x\rangle$ (g/cm^2)	Σ_R (μm)	Σ_B (μm)	$\Sigma_R/\langle x\rangle$	$\Sigma_B/\langle x\rangle$
0.1	25	0.45	0.013	0.12	0.17	0.27	0.38
1.0	40	13.9	0.42	2.7	4.7	0.19	0.33
5.0	50	94.1	2.82	10.8	20.8	0.12	0.22
10	65	201	6.04	15.7	33.2	0.08	0.17

Range straggling is defined by

$$\Sigma_R(E) = \sqrt{\langle x^2\rangle - \langle x\rangle^2}. \tag{13}$$

Beam blooming is defined by

$$\Sigma_B(E) = \sqrt{\langle y^2\rangle}. \tag{14}$$

Both Σ_R and Σ_B are evaluated numerically using Eqs. (10)–(12). Although the focus of this paper is on hydrogenic plasmas ($Z=1$), the strong Z dependence of scattering is directly reflected in the penetration, straggling, and blooming (Table I). In particular, with increasing Z the penetration $\langle x\rangle$, but not the total path length [$R=\int_{E_0}^{T_e}(dE/ds)^{-1}dE$], rapidly drops and the blooming effects ($\Sigma_B/\langle x\rangle$) notably increase. (The constancy in R is a result of the fixed n_e used for the calculations of Table I.) Figure 1 illustrates further details of Σ_R and Σ_B as 1-MeV electrons slow in a DT plasma, which demonstrate the importance of these effects as the electron energy degrades. As a consequence, an extended region of energy deposition occurs longitudinally ($\pm\sim 3$ μm) and lat-

TABLE IV. Interactions of 10 and 100-keV electrons with DT, Be, and plastic CH plasmas, common ablator or fuel materials of ICF. The plasma $T_e\sim 10$ eV. (For CH, the scattering effects are calculated for carbon ions and all plasma electrons).

E_0 (keV)		ρ (g/cm^3)	R (μm)	$\langle x\rangle$ (μm)	$\rho\langle x\rangle$ (g/cm^2)	Σ_R (μm)	Σ_B (μm)	$\Sigma_R/\langle x\rangle$	$\Sigma_B/\langle x\rangle$
10	DT	0.25	6.0	4.72	1.2×10^{-4}	1.09	1.60	0.23	0.33
		1.0	1.67	1.35	1.4×10^{-4}	0.31	0.44	0.23	0.32
	Be	1.85	0.84	0.57	1.1×10^{-4}	0.18	0.24	0.31	0.42
		7.4	0.23	0.16	1.2×10^{-4}	0.05	0.067	0.31	0.42
	CH	1.0	1.16	0.72	7.2×10^{-5}	0.26	0.35	0.36	0.48
		4.0	0.32	0.21	8.4×10^{-5}	0.076	0.10	0.36	0.48
100	DT	0.25	330	283	7.1×10^{-3}	42.8	75.4	0.15	0.27
		1.0	86.0	75.0	7.5×10^{-3}	11.1	19.1	0.15	0.26
	Be	1.85	43.0	31.0	5.7×10^{-3}	8.17	12.1	0.26	0.39
		7.4	11.3	8.5	6.2×10^{-3}	2.20	3.27	0.26	0.38
	CH	1.0	59.7	42.4	4.2×10^{-3}	13.6	17.2	0.32	0.41
		4.0	15.6	11.0	4.4×10^{-3}	3.57	4.49	0.32	0.41

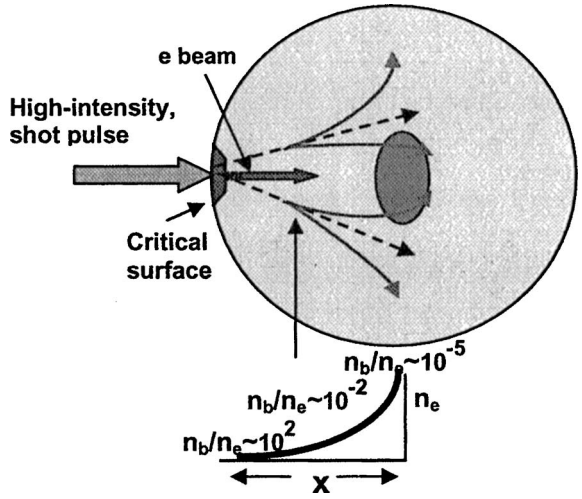

FIG. 3. Schematic illustration of beam blooming in a precompressed FI capsule. Two distinct regions for electron transport are illustrated: First, when $n_b/n_e > 10^{-2}$, the electron transport is highly filamented due to Weibel-like instabilities which dominate energy loss and beam blooming; however, for $n_b/n_e < 10^{-2}$, for which λ_D is clearly smaller than the energetic electron gyro radius associated with the beam current, the Weibel-like instabilities are stabilized and the electrons are then subject to the scattering, straggling, and blooming processes described herein. The dashed lines schematically indicate electron beam trajectories without the effects of blooming and straggling (see text).

erally ($\pm \sim 5$ μm) about the mean penetration, 13.9 μm for this case.

From a different point of view, Fig. 2 shows the effective enhancement of the stopping power in the extended region in which straggling and blooming are important. The combined effects of Σ_R and Σ_B will result in an asymmetric energy deposition region about the mean penetration. In contrast to an earlier work [10] these calculations inextricably link energy loss, straggling, and blooming. Thus the assumption of uniform energy deposition over the entire path length of the electron's trajectory [11] has only approximate justification.

The insensitivity of scattering effects ($\Sigma_R/\langle x\rangle$ and $\Sigma_B/\langle x\rangle$) and $\rho\langle x\rangle$ upon ρ is illustrated in Table II. This shows that density gradients, such as what would occur towards the core region of an actual FI experiment, will not impact the general scope of these calculations. The slight increase in $\rho\langle x\rangle$ with ρ simply reflects the slight decrease in the Coulomb logarithm of the stopping power [Eq. (9)] as ρ increases. Furthermore, these results are quite insensitive over a wide range in temperature [14].

Table III illustrates the enhancement of scattering effects ($\Sigma_R/\langle x\rangle$ and $\Sigma_B/\langle x\rangle$) as the electron energy decreases from 10 to 0.1 MeV. These effects are also important for the electron preheat problem [14], as shown in Table IV, but for regimes of lower energy (10–100 keV) and much lower density. Similar to Table I, $\Sigma_R/\langle x\rangle$ and $\Sigma_B/\langle x\rangle$ are seen to increase with the Z of the plasma, where the selected materials are common to those used, or contemplated for use at either OMEGA or the National Ignition Facility (NIF), for ablators and/or the fuel [4]. Focusing on the NIF, and direct drive scenarios, the DT ice thickness for the capsule is approximately 300 μm, which is very comparable to the penetration of 100 keV electrons. For present NIF indirect drive scenarios, the Be ablator of the capsule is $\sim$150 μm thick, which is $\sim$5 times larger than the penetration of 100 keV electrons. Finally the density jump assumed in the tables ($\approx$4) could, for example, reflect the effects of the passage of a strong shock. As illustrated in Table II for very different conditions, $\rho\langle x\rangle$ is again insensitive to the change in ρ, but $\langle x\rangle$ is notably affected.

Figure 3 shows a schematic representation of FI capsules. The relativistic electrons are generated by an intense laser interacting at the critical surface. As the electrons are initially transported, they are subject to Weibel-like instabilities [20,21] which can cause both spreading and energy loss in this region. However, for electrons that transport farther into the increased density portions of the capsule ($n_b/n_e < 10^{-2}$), Weibel-like instabilities are stabilized and the electrons then become subject to the scattering processes described herein. This stabilization can be understood since the gyro radius associated with the self-generated fields of the beam current is much larger than λ_D. This indicates the dominance of the binary interactions, and the motivation for exploring these processes in this paper. Thus in this regime, the interaction can be envisioned as the linear superposition of individual, isolated electrons interacting with plasma. Hence these scattering processes, which involve energy loss, straggling, and beam blooming become the ultimate mechanism that determines the details of energy deposition, whether in the dense core or outside, and therefore ultimately determine the effectiveness of capsule ignition. From a different point of view, the extent of beam blooming and straggling is critical for the FI target design since the finite size of the highly compressed core requires accurate understanding and control of the beam divergence which, if too severe, will preclude ignition.

In summary, from fundamental principles, the interaction of directed energetic electrons with hydrogenic and arbitrary-Z plasmas is analytically modeled. The effects of stopping, straggling, and beam blooming, a consequence of multiple scattering and energy loss, are rigorously treated from a unified approach. The sensitivity of these scattering effects, or the lack thereof, has been illustrated for several cases of different Z, densities, and initial electron energies, all of which span the range of relevance to many present and planned experiments. For fast ignition or electron preheat, enhanced energy deposition is found to be inextricably linked to beam blooming and straggling. These effects will, therefore, be important for evaluating the requirements of fast ignition and tolerable levels of electron preheat.

This work was supported in part by U.S. Department of Energy Contract No. DE-FG03-99SF21782, LLE Contract No. PO410025G, LLNL Contract No. B313975, and the Fusion Science Center for Extreme States of Matter and Fast Ignition Physics at University of Rochester.

[1] L. Spitzer, *Physics of Fully Ionized Gases* (Interscience, New York, 1962).
[2] B. Trubnikov, *Review of Plasma Physics 1* (Consultants Bureau, New York, 1965).
[3] C. K. Li and R. D. Petrasso, Phys. Rev. Lett. **70**, 3063 (1993).
[4] J. D. Lindl, *Inertial Confinement Fusion* (Springer-Verlag, New York, 1998).
[5] J. D. Lindl, R. L. McCrory, and E. M. Campbell, Phys. Today **45**(9), 32 (1992).
[6] S. Skupsky, Phys. Rev. A **16**, 727 (1977).
[7] C. K. Li and R. D. Petrasso, Phys. Rev. Lett. **70**, 3059 (1993).
[8] R. D. Petrasso, J. A. Frenje, C. K. Li, F. H. Séguin, P. B. Radha, C. Stoeckl, J. A. Delettrez, V. Yu. Glebov, D. D. Meyerhofer, and T. C. Sangster, Phys. Rev. Lett. **90**, 095002 (2003).
[9] M. Tabak, J. Hammer, M. Glinsky, W. L. Kruer, S. C. Wilks, J. Woodworth, E. M. Campbell, M. D. Perry, and R. J. Mason, Phys. Plasmas **1**, 1626 (1994).
[10] C. Deutsch, *et al.*, H. Furukawa, K. Mima, and K. Nishihara, Phys. Rev. Lett. **77**, 2483 (1996).
[11] S. Atzeni, Phys. Plasmas **6**, 3316 (1999).
[12] M. H. Key, M. D. Cable, T. E. Cowan, K. G. Estabrook, B. A. Hammel, S. P. Hatchett, E. A. Henry, D. E. Hinkel, J. D. Hilkenny, J. A. Koch, W. L. Kruer, A. B. Langdon, B. F. Lasinski, R. W. Lee, B. J. MacGowan, A. MacKinnon, J. D. Moody, M. J. Morgan, A. A. Offenberger, D. M. Pennington, M. D. Perry, T. J. Phillips, T. C. Sangster, M. S. Singh, M. A. Stoyer, M. Tabak, G. L. Tietbohl, M. Tsukamoto, K. Wharton, and S. C. Wilks, Phys. Plasmas **5**, 1966 (1998).
[13] C. Ren, M. Tzoufras, F. S. Tsung, W. B. Mori, S. Amorini, R. A. Fonseca, L. O. Silva, J. C. Adam, and H. Heron, Phys. Rev. Lett. **93**, 185004 (2004).
[14] C. K. Li and R. D. Petrasso, Phys. Rev. E **70**, 067401 (2004).
[15] M. D. Rosen, R. H. Price, E. M. Campbell, D. W. Phillion, K. G. Estabrook, B. F. Lasinski, J. M. Auerbach, S. P. Obenschain, E. A. McLean, R. R. Whitlock, and B. H. Ripin, Phys. Rev. A **36**, 247 (1987).
[16] *Beam and Jets in Astrophysics*, edited by P. A. Hughs (Cambridge University Press, Cambridge, 1991).
[17] H. W. Lewis, Phys. Rev. **78**, 526 (1950).
[18] N. F. Mott, Proc. R. Soc. London, Ser. A **135**, 429 (1932).
[19] C. Møller, Ann. Phys. **14**, 531 (1932).
[20] E. S. Weibel, Phys. Rev. Lett. **2**, 83 (1959).
[21] M. Honda, J. Meyer-ter-Vehn, and A. Pukhov, Phys. Rev. Lett. **85**, 2128 (2000).